Accurate Ellipsometric Magnetic-Field Sensor Used to Align the LNE Watt Balance Magnetic Circuit

K Ouedraogo, S Topsu, J Gayhmouni, L Chassagne, Y Alayli, Patrick Juncar, P Gournay, F Bielsa, G Geneves

Accurate Ellipsometric Magnetic-Field Sensor Used to Align the LNE Watt Balance Magnetic Circuit

K. Ouedraogo, S. Topsu, J. Gayhmouni, L. Chassagne, Y. Alayli

LISV/ University of Versailles, Versailles 78035 France.

P. Juncar, P. Gournay, F. Bielsa, G. Geneves

LCM/LNE-CNAM, Trappes 78190 France.

Abstract

Magnetic-field sensors based on the Faraday effect in a $Tb_3Ga_5O_{12}$ crystal are investigated in terms of their sensitivity, accuracy and directionality. The possibility of an increased sensitivity of such Faraday effect sensors due to the application of multipass sensitive elements is considered. Signal-to-noise measurements on 5 mm diameter × 20 mm long sample yield magnetic fields equivalent noise of 300 nT/Hz$^{1/2}$ ($\tau = 1$ s). The sensor has a sensitivity of 5.457(1) rad/T. Using spinning quarter waveplate ellipsometer, we can measure magnetic fields to 1 T. The data acquisition rate could be up to 80 Hz. This sensor is used to check the homogeneity and orientation of the field provided by the LNE watt balance magnetic circuit which the aim is to redefine the SI unit of mass in the near future.

PACS numbers: 42.81.Pa, 07.55.Ge

Keywords: Magnetometers for magnetic field measurements, Polarimetry, Watt balance, Metrology

I. INTRODUCTION

The Faraday-effect based sensors (FES) uses the Faraday rotation of the plane of polarized light travelling through a magnetic material. Numerous works are devoted to the development of FES for magnetic field and current measurements [1–7]. There exist two main types of such FESs: all-fiber sensors, in which a fiber serves as a transmitting medium and a sensitive element [8–10], and sensors with bulk sensitive elements, in which an optical fiber is used for signal transmission and a material with magneto-optic properties serves as a sensitive element [11–13]. Examples of such materials are paramagnetic crystals, ferrite garnet films [14–18], diamagnetic glasses [19], and $Bi_{12}GeO_{20}$ and $Bi_{12}SiO_{20}$ crystals [20]. In comparison with conventional transformer sensors, FESs exhibit numerous advantages. The main ones are the passive character of sensitive elements, the absence of an electric power supply, the noise immunity, the small dimensions, and the possibility of remote measurements at a relatively high sensitivity and efficiency [21]. Furthermore, there are two basic kinds of magnetic sensors : vector magnetometers that measure the components of the magnetic field and scalar magnetometers that measure the magnitude of the magnetic field. In this paper, we describe the realization of a vector magnetometer based on the Faraday effect combined with an ellipsometer. Our device has a wide range of measurement and a high resolution. This sensor is dedicated to check the homogeneity and the magnetic field orientation axis of the LNE watt balance magnetic circuit which aim is to redefine the SI unit of mass in the near future by linking it to the Planck constant.

II. PRINCIPLE OF THE POLARIMETRIC MAGNETIC FIELD SENSOR

The Faraday effect results from the fact that the crystal's index of refraction is different if the electrons precess about the longitudinal magnetic field in the same or in the opposite sense as the rotation of the electric field of the circularly polarized light. A figure of merit used to compare this effect between materials is the Verdet constant V, which has units of angular rotation per unit of applied field per unit of material length. For a crystal in the presence of the magnetic flux density, the total circular birefringence consists of natural birefringence and field-induced birefringence. A common magneto-optic material for field sensing is terbium gallium garnet $Tb_3Ga_5O_{12}$ crystals. It has a large Verdet constant, low light loss, high thermal conductance and high light damage threshold. In perfect $Tb_3Ga_5O_{12}$ crystals, natural linear birefringence is absent because these crystals have a cubic symmetry and are isotropic. Hence, the rotation angle of the polarization plane for a light wave that passes through the crystal under an external magnetic flux density is given by

$$\psi = (VB \times \sin(\alpha) + \Theta)L \tag{1}$$

where V is the Verdet constant of the $Tb_3Ga_5O_{12}$ crystal which is equal to 134 rad/(T.m) at 632.991 nm, $B \times \sin(\alpha)$ is the projection of the external magnetic flux density along the direction of the light-wave propagation in the crystal, L is the length of the crystal and Θ is the coefficient of natural optical activity of the $Tb_3Ga_5O_{12}$. The effect is largest when the propagation direction of the light, the crystal axis, and the applied magnetic field are all aligned. The most common method for measuring ψ consists of using the Malus law, *i.e.* to link the value of B to the intensity of the light wave at the output of the device. In this case the power stability of the light source is a key parameter for the accuracy of the sensor.

In our setup, the output beam is sent into a polarimeter that measures the ellipsometric parameters (ψ, Δ) of the laser beam [22] leading to a more accurate and less power sensitive device. Figure 1 gives a schematic view of our ellipsometric sensor of magnetic field.

An output fibered He-Ne laser is used as a laser source. A Glan-Thompson polarizer, placed at the output of the optical fiber, reduces the systematic error induced by the use of a partially polarized laser source. A 5 mm diameter $\times$ 20 mm long crystal of $Tb_3Ga_5O_{12}$ is used as a Faraday sensitive element. The rear surface of the crystal is mirror coated in order to use it in a double-pass configuration. Once travelling into the crystal, the laser beam is passed sequentially through a rotating quarter waveplate and a fixed polarizer which transmits a beam whose intensity varies as a function of the rotational angle of the plate. The transmitted beam is sent upon a photodetector which produces an electric signal proportional to the intensity of the transmitted light. The rotating quarter waveplate cyclically varies the polarization of the beam. The electrical signal, when numerically Fourier analyzed, provides Fourier coefficients having both phase terms and amplitude terms of the parallel (ξ_p) and perpendicular (ξ_s) components of the electric vector of the polarized reflected beam [22]. From these terms, the ellipsometric parameter Δ is deduced from the instantaneous phase difference between both components leading to the terms $\sin(\Delta)$ and $\cos(\Delta)$. Therefore, the phase difference Δ is uniquely and unambiguously defined in a single measurement. Since the ellipsometric parameter ψ is also uniquely defined by $\tan\psi = |\xi_p| \,/\, |\xi_s|$, the amplitude of the components issue from the Fourier analysis of the laser beam could also permit to determine the orientation of the polarization plane of the laser beam.

The measurement of ψ could be done over 2π rad. Using eq. (1), the measurement range of such device could theoretically be as large as from 3 μT to 1 T. Notice that if the value of the measured magnetic density flux is estimated approximately close to 1 Tesla, the

measurement range could be larger as the value of ψ is given modulo 2π.

III. EXPERIMENTAL CALIBRATION OF THE SENSOR

A. Resolution of the device

One of the main parameters that need to be characterized is the resolution of our device defined as the root mean square of the noise level. In order to estimate this parameter, the output signal of the sensor is recorded over several hours for a fixed input polarization state and no magnetic flux density. The surrounding parameters, the room temperature (PT100 thermistor - $1\sigma = 5$ mK), the room pressure (Digiquartz, Paroscientifics - $1\sigma = 3$ Pa), the humidity content (MH4, General Eastern - $1\sigma = 1$ %), are controlled during the acquisition time in order to limit systematic errors. We use the Allan standard deviation [23] as a mathematical operator to estimate the instability level of ψ due to noise processes. It is expressed as

$$\sigma_y^2(\tau) = \frac{1}{2(K-1)} \sum_{i=0}^{K-2} (\overline{\psi_{i+1}}(\tau) - \overline{\psi_i}(\tau))^2 \tag{2}$$

where $\overline{\psi_i}$ the normalized value of each measurement point of the K samples. A number of 3200 samples have been recorded. The samples are taken with no dead-time between them. The result is reported in Figure 2. We obtain a noise level of σ_y=9.97$\times 10^{-6}$ rad for a data acquisition rate of 80 Hz. Using eq.(1), this corresponds to a resolution of σ_y=2.7 μT/$\sqrt{\text{Hz}}$. Since the total noise power is a function of measurement bandwidth, the value of the resolution is typically given for τ=1 s. For an integration time of τ=1 s, we reach a value of σ_y=300 nT/$\sqrt{\text{Hz}}$. The Flicker noise is achieved for $\tau = 10$ s which leads to a minimal resolution of the sensor of 1σ=120 nT.

B. Sensitivity of the device

The sensitivity of the sensor is defined as the quotient of the change in the polarization plane of the laser beam and the corresponding change in a value of a magnetic flux density. Hence, the theoretical sensitivity of the sensor is defined as

$$S = \frac{\partial \psi}{\partial B} = 2VL. \tag{3}$$

With our configuration, eq. 2 gives a theoretical value of S_{th}=5.80 rad/T. To determine experimentally the sensitivity of our device, we built an electromagnet. The magnetic flux density created by the electromagnet is proportional to both the number of turns in the winding N_S and the current I in the wire. So

$$\overrightarrow{B} = \mu_0 \times N_S \times I \times \overrightarrow{u}_z \tag{4}$$

where $\mu_0 = 4\pi \times 10^{-7}$ H.m^{-1} is the magnetic permeability in air. Taking into account the limit of thermal dissipation possible with our electromagnet, the maximum current is 6 A leading to a magnetic flux density range of [0-24 mT]. The magnetic flux density generated by the electromagnet is measured by a Hall effect sensor (Model 6010, F.W.Bell) with a resolution of 100 nT/$\sqrt{\text{Hz}}$ (τ=1 s), a measurement range of [0-300 mT] and an accuracy of 2% of the nominal value. As the Hall effect sensor is a vector magnetometer that measures the components of the magnetic field, the sensor is adjusted in order to maximize the signal at the center of the electromagnet. Our ellipsometric magnetometer, which is also a vector magnetometer, is placed in front of the Hall effect sensor as illustrated in Figure 3. Simultaneously, the value of both sensors are recorded onto a data acquisition

board as a function of the current into the electromagnet.

Figure 4 reports the output curves of both sensors, $\partial B/\partial I$ for the Hall effect sensor and $\partial\psi/\partial I$ for the ellipsometric sensor. The slopes of the curves are respectively, $2.54(5)\times10^{-2}$ rad.A^{-1} and 4.668(84) mT.A^{-1}. Combining both values, we obtain

$$S = \frac{\partial\psi}{\partial B} = \frac{\partial\psi}{\partial I} \times \frac{\partial I}{\partial B} = 5.4573\ rad/T. \tag{5}$$

Let α_1 and α_2 be equal to respectively $\partial\psi/\partial I$ and $\partial B/\partial I$. The uncertainty on the sensitivity is deduced from the variance, expressed by

$$V(S) = \sum_{i=1}^{i=2} \left(\frac{\partial S}{\partial \alpha_i}\right)^2 V(\alpha_i) + 2\sum_{i=1}^{i=2}\sum_{j=1}^{j=2} \frac{\partial S}{\partial \alpha_i}\frac{\partial S}{\partial \alpha_j} cov(\alpha_i, \alpha_j). \tag{6}$$

As the two parameters α_1 and α_2 are independent, $\forall(i,j)\ cov(\alpha_i, \alpha_j) = 0$ and eq. 5 becomes

$$V(S) = \alpha_2^{-2} V(\alpha_1) + \alpha_1^2 \alpha_2^{-4} V(\alpha_2). \tag{7}$$

Taking the square root of eq. 6, we obtain an uncertainty of $\pm10^{-3}$ rad.T^{-1} on the mean value of the sensitivity, hence S=5.457(1) rad/T. Although this value is in agreement with the theoretical value calculated previously a discrepancy is observed. This bias error could be explained by the uncertainty on the Verdet constant, an imperfect alignment between the principal axis of the sensors and the magnetic field of the electromagnet.

IV. APPLICATION TO THE LNE WATT BALANCE MAGNETIC CIRCUIT

The SI unit of the mass defined since 1889 by an artefact, is devoted to change because of its lake of perenniality [24]. Several projects are under way for this purpose [25–29]. One of these projects, called the watt balance, has been initially proposed by B. P. Kibble of the UK National Physical Laboratory in 1975. The principle of the watt balance has been extensively described in several papers [30, 31]. It consists of a two-parts experiment in which electrical and mechanical powers are compared. Firstly, a standard mass m is weighed against a Laplace force produced by a current i flowing in a coil of length L located in a magnetic flux density B within the air-gap of a magnetic circuit. Secondly, the coil is moved through the same magnetic field at a known speed v. By Faraday's law of induction, a potential difference ξ is generated across the ends of the wire. Considering the overall experiment, we reach an equivalence between electrical and mechanical powers expressed as $mgv = \xi i$. Accurate measurements of electric current and potential difference are based on values of the Josephson constant, the von Klitzing constant and the Planck constant. Hence, the watt balance would become an instrument to measure a mass and even to redefine the unit of mass if the value of the Planck constant is determined definitely [32, 33].

The design of the magnetic circuit is fully detailed in [34]. It is an axis-symmetric circuit composed of a Sm_2Co_{17} magnet ring and two pure iron yokes concentrating the flux in an 85 mm height and 9 mm thick air-gap. The mean value of the magnetic flux density $\overrightarrow{B}$ at its center is about 1 T. The air-gap shape has been optimized to obtain the higher possible radial flux density (Br) with a relative variation of less than $\pm 10^{-4}$ along the useful vertical path of the air-gap, the vertical flux density component (Bz) being kept below $\pm 10^{-4}$ of the radial component.

Figure 5 gives a general view of the mechanical mount built specifically to align and to adjust our ellipsometric sensor in the air gap of the magnetic circuit of the LNE watt balance. A motorized rotation stage allows to rotate the magnetic circuit. A linear motor is used to control the vertical position (z axis) of the $Tb_3Ga_5O_{12}$ crystal in order to measure with our FES the variation of the ratio Bz/Br using a nominal value of Br given by [34]. This ratio will permit to check the homogeneity and the orientation of the magnetic flux density. The edge of our FES other Hall effect sensors is that we can use a laser beam to align the sensor in regard to the gravity axis $\overrightarrow{g}$ thanks to a level sensor (Nivel20, Leica) and autocollimation method. The revolution axis of the magnetic circuit, which has to be parallel to $\overrightarrow{g}$, is optimized by minimizing the value of ψ given by our sensor.

We report on Figure 6 the variation of the ratio Bz/Br to check the homogeneity of $\overrightarrow{B}$ and locate its revolution axis. Reported results have been done for two vertical positions (30 mm and 42 mm) in the air gap of the magnetic field of LNE watt balance. For both positions, the ratio Bz/Br are less than $\pm 10^{-4}$ and seems to be in agreement with the specifications of the watt balance project. The rotation of the magnetic circuit around its revolution axis shows periodical variations due to the incline of the magnetic flux density in regard to a horizontal position. These variations will be used as a parameter for the alignment of the magnetic field of the LNE watt balance with a resolution at best of 300 nrad. Although these preliminary results are promising, further measurements are in progress.

V. CONCLUSION

We developed an accurate FES sensor based on the use of a spinning quarter waveplate ellipsometer. Our device demonstrated a resolution of 300 nT/$\sqrt{\text{Hz}}$ (τ=1 s), a sensitivity of 5.457(1) rad/T and a range measurement up to 1 T. This sensor has been used to check the

homogeneity and the revolution axis of the LNE watt balance magnetic circuit. We plan to improve the mechanic-holder of the sensor to be less sensitive to mechanical vibrations in order to increase the integration time without deteriorating the resolution of the device.

---

[1] R.S. Popovic, J.A. Flanagan, P.A. Besse, The future of magnetic sensors, Sens. Actuators A 56, (1996) 39-55.

[2] A. Edelstein, Advances in magnetometry, J. Phys: Condens. Matter. 19, (2007) 28.

[3] P. Ripka, Magnetic sensors and magnetometers, Artech House, London, 2000.

[4] C. Schott, H. Blanchard, R.S. Popovic, R. Racz, J. Hrejsa, High accuracy analog Hall probe, IEEE. Trans. Instr. Meas. 46, (1997) 613-616.

[5] A.B. Villaverde, E. Munin, C.B. Pedroso, Linear displacement sensor based on the magneto-optical Faraday effect, Sens. Actuators A 70, (1998) 211-218.

[6] S. A. Oliver, C. A. DiMarzio, S. C. Lindberg, A. B. Kale, Magnetic field measurements using magneto-optic Kerr sensors, Opt. Eng. 33, (1994) 3718-3722.

[7] M. Bock, R. Umathum, J. Sikora, S. Brenner, E.N. Aguor, W. Semmler, Faraday effect position sensor for interventional magnetic resonance imaging, Phys. Med. Bio. 51, (2006) 999-1009.

[8] A.J. Rogers, Optical-fibre current measurement, Int. J. Optoelectron. 3, (1988) 391–407.

[9] A.J. Rogers, Optical measurement of current and voltage on power systems, IEE J. Electr. Power Appl. 12, (1979) 120.

[10] K.P. Koo, F. Bucholtz, D.M. Dangenais, A. Dandridge, A compact fiber-optic magnetometer employing an amorphous metal wire transducer, IEEE Photonics Technol. Lett. 1, (1989) 464.

[11] R.L. Patterson, A.N. Rose, D. Tang, G.W. Day, A fiber-optic current sensor for aerospace applications, IEEE Aerospace and Electron. Syst. Mag. 5, (1990) 10.

[12] V.K. Gorchakov, V.V. Kutzaenko, V.T. Potapov, Electrooptical and magnetooptical effects in bismuth silicate crystals and polarization sensors using such crystals, Int. J. Optoelectron. 5, (1990) 235.

[13] Y. Yamagata, T. Oshi, H. Katsukawa, S. Kato, Y. Sakurai, Development of optical current transformers and application to fault location systems for substations, IEEE Trans. Power Deliv. 8, (1993) 866.

[14] O. Kamada, H. Minemoto, S. Ishizuka, Mixed rare-earth iron garnet (TbY) IG for magnetic field sensors, J. Appl. Phys. 61, (1987) 3268.

[15] M.N. Deeter, A.H. Rose, and G.W. Day, Fast sensitive magnetic-field sensors based on the Faraday effect in YIG, J. Lightwave Technol. 8, (1990) 1838-1842.

[16] A.H. Rose, M.N. Deeter, G.W. Day, Submicroampere-per-root-hertz current sensor based on the Faraday effect in Ga: YIG, Opt. Lett. 18, (1993) 1471-1473.

[17] K.V. Rochford, A.N. Rose, G.W. Day, Magneto-optic sensors based on iron garnets, IEEE Trans.Magn. 32, (1996) 4113-4117.

[18] K. Kyuma, M. Shuichi Tai Nunoshita, T. Takioka, Y. Ida, Fiber optic measuring system for electric current by using a magnetooptic sensor, IEEE J.Quantum Electron. 18, (1982) 1619-1623.

[19] E.A. Ulmer, A high-accuracy optical current transducer for electric power systems, IEEE Trans. Power Delivery 5, (1990) 892.

[20] H. Takada, S. Miymoto, T. Mitsui, T. Tomimasu, Application of fibre-optic magnetic-field sensor to kicker magnet, J. Phys. E: Sci. Instrum. 21, (1988) 371.

[21] O. Kamada, T. Nakaya, S. Higuchi, Magnetic field optical sensor using Ce:YIG single crystals as a Farady element, Sens. Actuators A 119, (2005) 345-348.

[22] R.M.A. Azzam, N.M. Bashara, Ellipsometry and polarized light, Elsevier, Amsterdam, 1989.

[23] D. Allan, Statistics of atomic frequency standards, Proceed. IEEE 54**,** (1966) 221-230.

[24] R. Davis, The SI unit of mass, Metrologia 40, (2003) 299-305.

[25] G. Genevès, P. Gournay, A. Gosset, M. Lecollinet, F. Villar, P. Pinot, P. Juncar, A. Clairon, A. Landragin, D. Holleville, F. Pereira Dos Santos, J. David, M. Besbes, F. Alves, L. Chassagne, and S. Topçu„ The BNM Watt balance project, IEEE Trans. Instrum. Meas. 54, (2005) 850-853.

[26] P. Becker, M. Gläser, Avogadro constant and ion accumulation: steps towards a redefinition of the SI unit of mass, Meas. Sci. Technol. 14, (2003) 1249-1258.

[27] W. Beer, A.L. Eichenberger, B. Jeanneret, B. Jeckelmann, A.R. Pourzand, P. Richard, J.P.S chwarz, Status of the METAS watt balance experiment, IEEE Trans. Instrum. Meas. 52, (2003) 626-630.

[28] R. L. Steiner, E. R. Williams, R. Liu, D. B. Newell, Uncertainty Improvements of the NIST Electronic Kilogram, IEEE Trans. Instrum. Meas. 56, (2007) 592–596.

[29] A. Picard, M. Stock, H. Fang, T.J. Witt, D. Reymann, The BIPM Watt Balance, IEEE Trans. Instrum. Meas. 56, (2007) 538-542.

[30] B.P. Kibble, J.H. Sanders, A.H. Wapstra, Atomic Masses and Fundamental Constants, Plenum, New York, 1975.

[31] B.P. Kibble, L.A. Robinson, Replacing the kilogram, Meas. Sci. Technol. 14, (2003) 11243-1248.

[32] B.N. Taylor, T.J. Witt, New international electrical reference standards based on the Josephson and Quantum Hall Effects, Metrologia 26**,** (1989) 47-62.

[33] I.A. Robinson, B.P. Kibble, An initial measurement of Planck's constant using the NPL Mark

II watt balance, Metrologia 44, (2007) 427–440.

[34] P. Gournay, G. Genevès, F. Alves, M. Besbes, F. Villar, J. David, Magnetic circuit design for the BNM watt balance experiment, IEEE Trans. Instr. Meas. 54, (2005) 742-745.

FIGURE CAPTIONS

Figure 1 Optical scheme of the ellipsometric double-pass Faraday effect sensor. 1 output fibered laser source - 2 Glan-Tomphson polarizer - 3 beamsplitter - 4 hollow tube- 5 sensitive element - 6 mirror coating - 7 spinning quaterwave plate - 8 Polarizer - 9 Photodetector

Figure 2 Experimental result of the noise level.

Figure 3 Experimental setup used for the calibration of the ellipsometric sensor. 1 Photodetector 2 Polarizer - 3 Spinning quarter waveplate - 4 Beamsplitter - 5 Glan-Thompson polarizer - 6 Magnetic sensitive element - 7 Electromagnet - 8 Hall probe

Figure 4 Experimental measurements of the ratios $\partial\psi/\partial I$ issue from our FES ($\square$) and $\partial B/\partial I$ issue from the Hall probe ($\triangle$).

Figure 5 Schematic view (left) and photography (right) of the characterizing setup of the LNE watt balance magnetic circuit. 1 Vertical translation stage - 2 Horizontal translation stage - 3 Faraday sensor - 4 Magnetic circuit - 5 Rotation stage

Figure 6 Experimental measurements of the variations of the ratio Bz/Br (10^{-5}) in the air-gap of the magnetic circuit for two vertical positions (z=30 mm ($\square$) and z=42 mm ($\triangle$)).

Figure1

Click here to download high resolution image

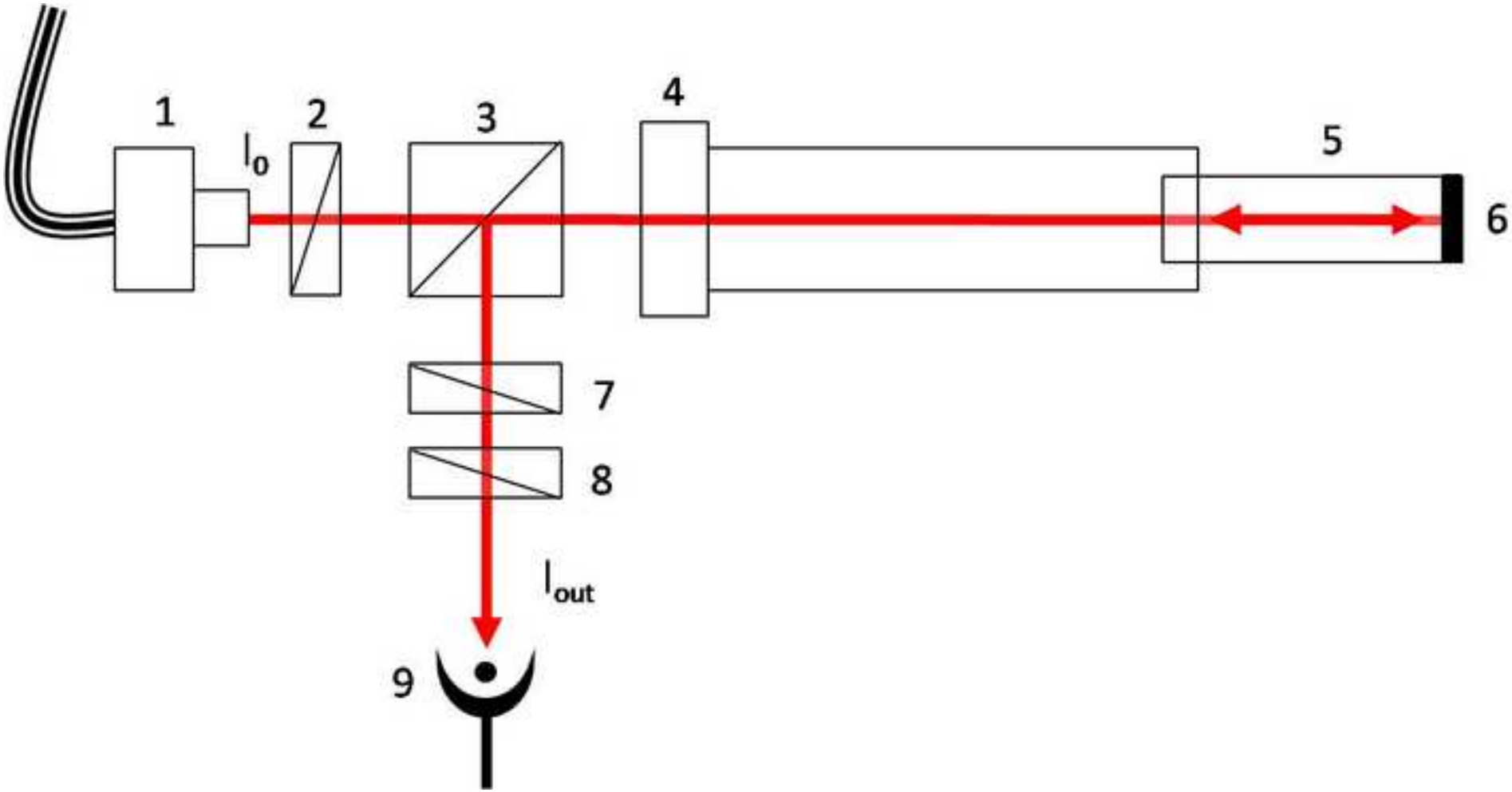

Figure2

Click here to download high resolution image

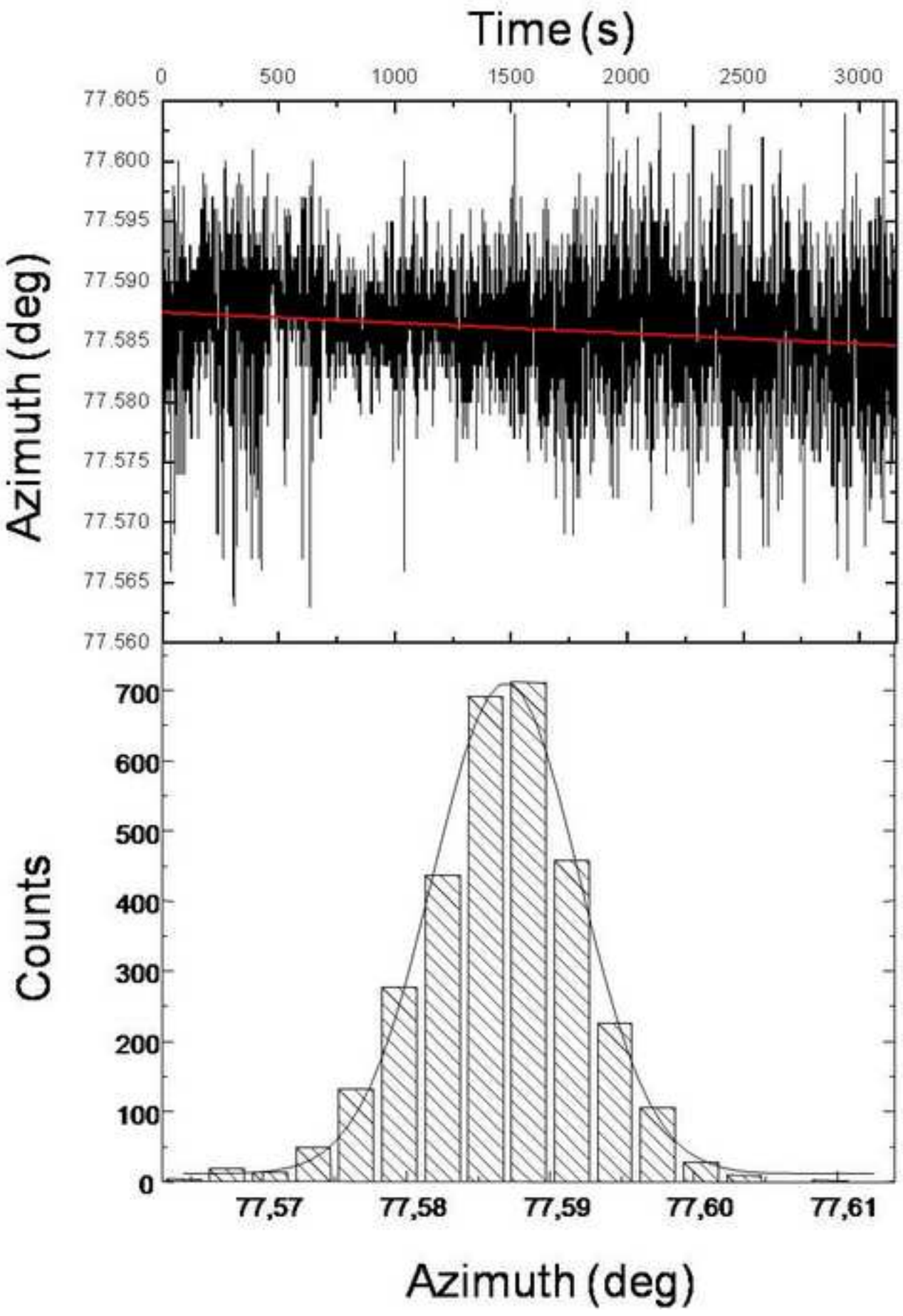

Figure3

Click here to download high resolution image

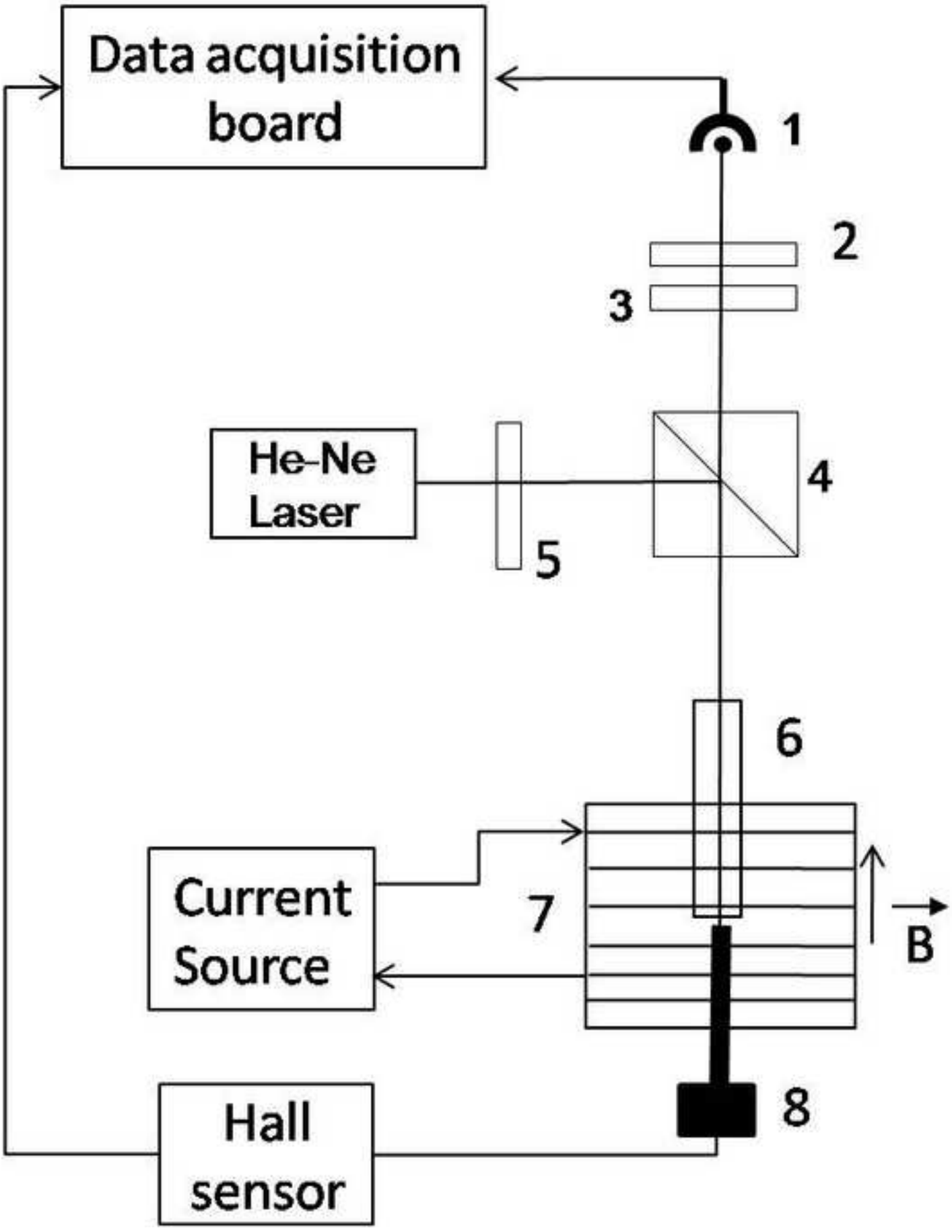

Figure4

Click here to download high resolution image

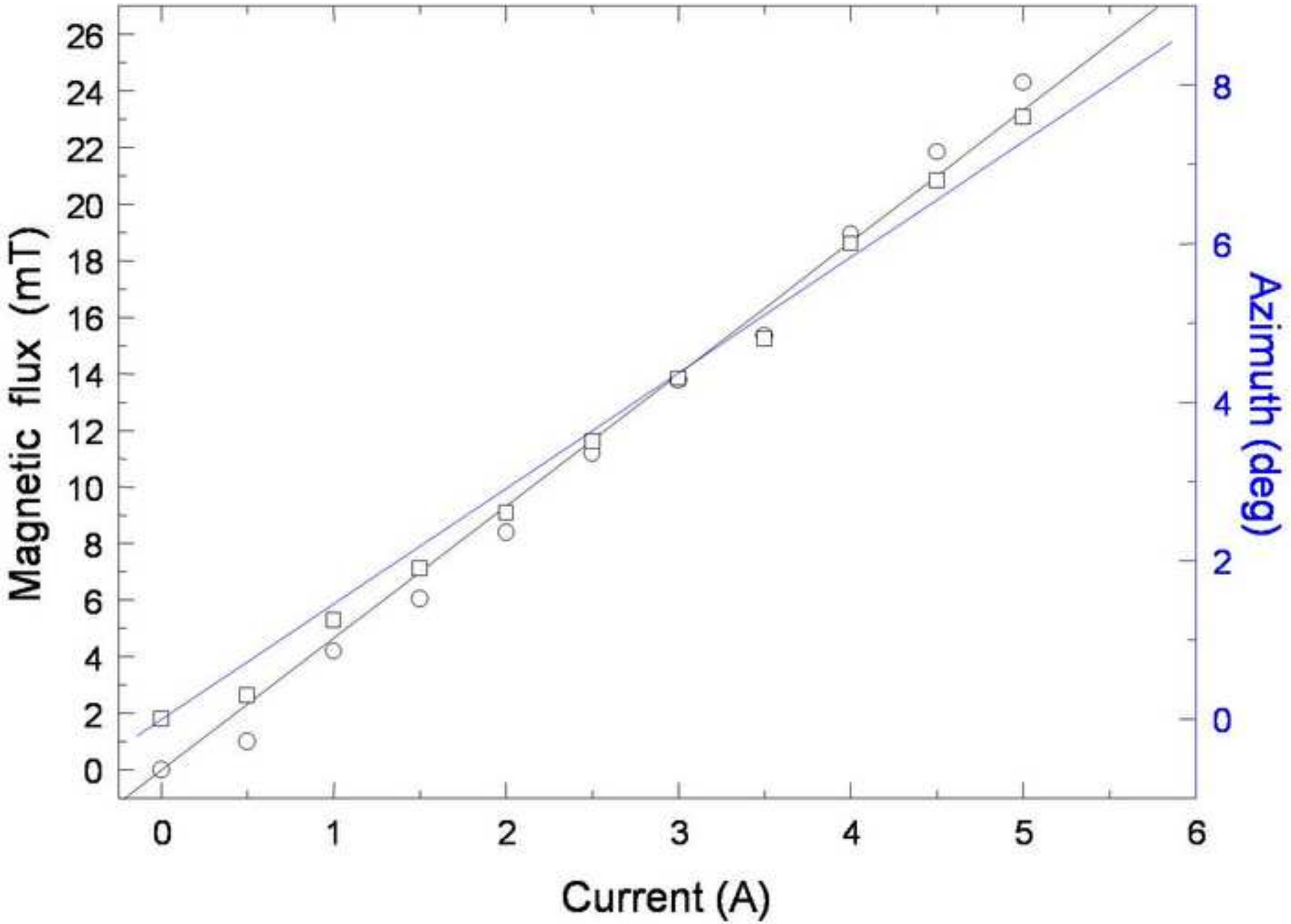

Figure5

Click here to download high resolution image

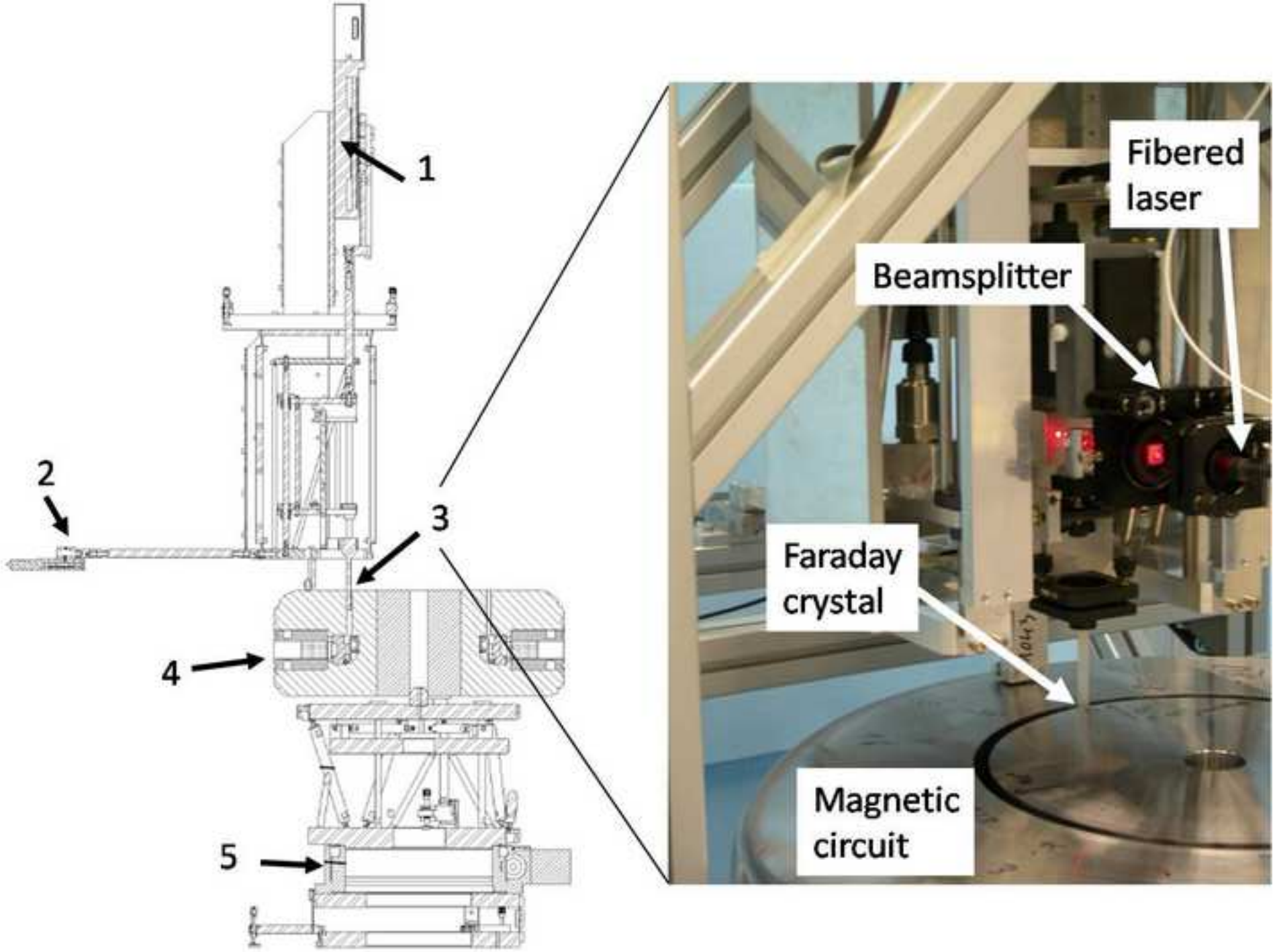

Figure6

Click here to download high resolution image